Osteoarthritis and Cartilage 20 (2012) 1011–1019

Osteoarthritis and Cartilage

OARSI OSTEOARTHRITIS RESEARCH SOCIETY INTERNATIONAL

High resolution micro arthrography of hard and soft tissues in a murine model

X.I. Gu †‡[a], P.E. Palacio-Mancheno †[a], D.J. Leong ‡§‖, Y.A. Borisov †, E. Williams †, N. Maldonado †, D. Laudier ‖, R.J. Majeska †‡, M.B. Schaffler †‡, H.B. Sun §‖, L. Cardoso †‡*

† *Department of Biomedical Engineering, The City College of New York of The City University of New York, NY 10013, USA*
‡ *The Graduate Center of The City University of New York, NY 10016, USA*
§ *Albert Einstein College of Medicine, Bronx, NY 10461, USA*
‖ *Mount Sinai School of Medicine, NY 10021, USA*

ARTICLE INFO

Article history:
Received 16 September 2011
Accepted 14 May 2012

Keywords:
Micro arthrography
Micro computed tomography
Contrast agent
3D Cartilage morphology
Murine knee joint
Surgical destabilization of the medial meniscus

SUMMARY

Objective: Recent developments on high resolution micro computed tomography (μCT) allow imaging of soft tissues in small animal joints. Nevertheless, μCT images cannot distinguish soft tissues from synovial fluid due to their similar mass density, limiting the 3D assessment of soft tissues volume and thickness. This study aimed to evaluate a lead chromate contrast agent for μCT arthrography of rat knee joints *ex vivo*.

Design: Intact tibiofemoral rat joints were injected with the contrast agent at different concentrations and imaged using a μCT at 2.7 μm isotropic voxel size. Cartilage thickness was measured using an automated procedure, validated against histological measurements, and analyzed as a function of μCT image resolution. Changes in hard and soft tissues were also analyzed in tibiofemoral joints 4 weeks after surgical destabilization of the medial meniscus (DMM).

Results: The contrast agent diffused well throughout the whole knee cavity without penetrating the tissues, therefore providing high contrast at the boundaries between soft tissues and synovial fluid space. Thickness analysis of cartilage demonstrated a high similarity between histology and μ-arthrography approaches ($R^2 = 0.90$). Four weeks after surgical DMM, the development of osteophytes (Oph) and cartilage ulcerations was recognizable with μCT, as well as a slight increase in trabecular bone porosity, and decrease in trabecular thickness.

Conclusions: A lead chromate-based contrast agent allowed discriminating the synovial fluid from soft tissues of intact knee joints, and thus made possible both qualitative and quantitative assessment of hard and soft tissues in both intact and DMM tibiofemoral joints using high resolution μCT.

Introduction

Joint diseases are characterized by a progressive degradation of joint tissues, abnormal matrix composition and altered cell metabolism[1,2]. These diseases are associated with soft tissue breakdown, as well as changes in hard tissues such as subchondral bone[3,4]. In addition to systemic factors, altered local biomechanics may lead to morphological changes in joint tissues that are indicative of loss of function and homeostasis. Moderate loads prevent cartilage degradation[5,6], in contrast to excessive loads, which cause cartilage to break down[7,8,9,10,11,12,13,14]. However, the relationship between biomechanics and biological mechanisms in joint tissues is not fully understood, and the need to investigate the cellular, molecular and biomechanical mechanisms behind these diseases has motivated the development of small animal models of joint degeneration[15,16,17].

The assessment of morphological changes in small animal joints is often performed using 2D histomorphometry, or with the help of modern imaging modalities such as micro-Magnetic Resonance Imaging (μMRI), micro-Computed Tomography (μCT), and Optical Coherence Tomography (OCT). However, quantitative assessment of changes in small animal joints is limited by the resolution and contrast of current 3D imaging approaches. μMRI offers excellent sensitivity for imaging soft tissues such as cartilage, ligaments, and tendons. However, the resolution of μMRI is in the order of 50 μm[18,19], which is not sufficient to appropriately characterize the morphology of cartilage in rats and mice[20,21,22]. OCT is capable of

* Address correspondence and reprint requests to: L. Cardoso, Department of Biomedical Engineering, The City College of The City University of New York, Steinman Hall T-565, 140th Street and Convent Ave, NY 10031, USA. Tel: 1-212-650-7154; Fax: 1-212-650-6727.
E-mail address: cardoso@engr.ccny.cuny.edu (L. Cardoso).
[a] Authors contributed equally to this study.

1063-4584/$ – see front matter © 2012 Osteoarthritis Research Society International. Published by Elsevier Ltd. All rights reserved.
doi:10.1016/j.joca.2012.05.004

imaging rat cartilage at high resolution[23,24,25], but generally provides two-dimensional (2D) images of the tissue[26] and its penetration depth is limited in whole knee joints. In turn, μCT allows acquiring high resolution images of the complete joint, but μCT is only considered appropriate to delineate hard tissues, as it exhibits poor sensitivity to discriminate materials with similar low mass densities (e.g., soft tissues and synovial fluid).

Despite recent progress in these imaging approaches, it remains challenging to acquire soft tissue images at resolutions capable of distinguishing changes in morphology and tissue composition in intact whole joints through a single imaging modality. The goal of this study was to evaluate the ability of a lead-chromate based contrast agent to improve the distinction and characterization of both hard and soft tissues in the rat tibiofemoral joint using high resolution μCT. By these means we aimed to: (1) improve the low image contrast between synovial fluid and soft tissues of μCT scanning on small animal joints, (2) investigate the role of images resolution on the quantitative assessment of cartilage thickness and volume, and (3) characterize changes in both hard and soft tissues in an osteoarthritis (OA) animal model induced via surgical destabilization of the medial meniscus (DMM).

Materials and methods

Contrast agent concentration

Microfil, a lead-chromate based contrast agent (FlowTech, Carver, MA), is generally used for producing casts of tissue's vasculature. The lead-chromate is bound to a silicon monomer that requires being mixed with a curing agent (hardener) to polymerize, thus producing a solid aggregate of the 3D vasculature tree. Due to the large size of the silicon-lead chromate molecule, the mixture does not diffuse across blood vessel walls or other soft tissues membranes; moreover, a diluent may be used for better penetration into smaller vessels (MV-Diluent). In this study, Microfil was used to fill out the space of the synovial fluid in the knee joint without diffusing into the cartilage or other soft tissues and to make the synovial fluid space to become X-ray dense. Therefore, the high contrast between the synovial space, soft tissues and bone will allow a clear depiction of the contour and volume of soft tissue morphology.

Segmentation of the scanned tissues and contrast agent was performed based on the different X-ray absorption by the material/tissue densities. Therefore, we carried out a quantitative test to determine the X-ray absorption (attenuation) of Microfil at different densities and dilutions. Two sets of Microfil solutions were prepared at different densities. The first solution, here referred as High Density Microfil (HDM), was concentrated by centrifugation at 10,000 rpm for 10 min, which produce three distinctive regions, a dense concentrate in the bottom, an intermediate fluid in the middle and a clear supernatant in the top. Fifty percent of the volume was removed from the top of the solution and the left 50% was rehomogenized using a pipette and a vortex for 5 min. The second solution, designated as Low Density Microfil (LDM), corresponded to the original concentration provided by the Microfil vendor. Both HDM and LDM were diluted at a ratio of 1:0, 1:1, 1:3 and 1:4 with the MV-Diluent and scanned with and without adding the curing agent.

Air, water and two hydroxyapatite (HA) phantoms of known density (250 and 750 mg/cm^3, 4 mm diameter) were scanned at 2.7 μm. HDM and LDM dilutions with and without hardener were reconstructed and separate volumes of interest (VOI) were created for each sample. A VOI was also obtained from two scans of the rat knee joint where 1:0 HDM and 1:0 LDM were used, corresponding to a region of the femoral condyle that included Microfil (synovial space), cartilage and subchondral bone. For each VOI, a histogram of intensity (Fig. 1), corresponding to the X-ray absorption was then analyzed using CT analyzer (CTAn) software (V1.11.0 Skyscan, Belgium). Image intensity is reported in Hounsfield Units (HUs), so that the values for air and water are −1000 HU and 0 HU respectively.

Intact and surgical DMM

The right hind limbs of 5 month old female Sprague Dawley rats were dissected after euthanasia using CO_2 in accordance to the Institutional Animal Care and Use Committee (IACUC) procedures

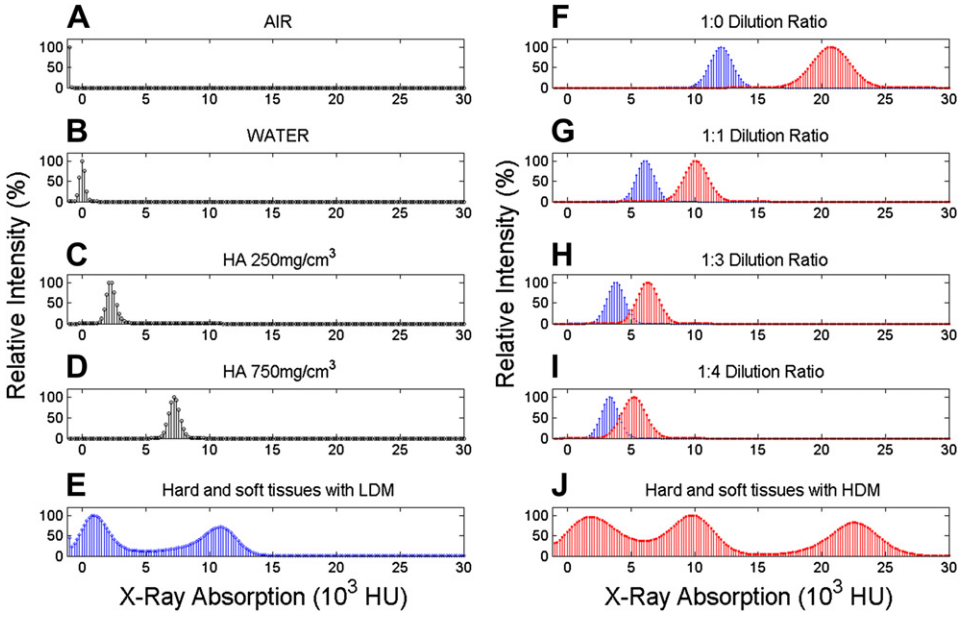

Fig. 1. On the left side, histograms of X-ray absorption in HUs for (A) air, (B) water, (C) 250 mg/cm^3 HA phantom, (D) 750 g/cm^3 HA phantom. On the right side, histograms represent (F) 1:0 LDM and HDM dilutions (G) 1:1 LDM and HDM dilutions, (H) 1:3 LDM and HDM dilutions, (I) 1:4 LDM and HDM dilutions. Bottom row indicates histograms of VOI of knee joint for (E) soft and hard tissues injected with 1:0 LDM, and (J) soft and hard tissues injected with 1:0 HDM.

at Mount Sinai School of Medicine. Hind limbs were cleaned free of muscle and both femur and tibia were cut at the mid-diaphysis, maintaining the knee joint intact. These samples were divided into two groups. In the first group ($n = 6$), 1:0 LDM without hardener was injected into the synovial cavity at the anterior, posterior, medial, and lateral compartments of the knee using a hypodermic 24 gauge needle. For each injection, approximately 3–5 ml of Microfil were used to make sure the synovial capsule was completely filled up with the contrast agent. After each injection, the knee joint was gently bent in flexion/extension to distribute and homogenize the contrast agent in the synovial cavity. Most contrast agent egresses trough the holes made in the synovial capsule by previous injections, and the volume that remains inside the knee is less than 1 ml approximately. This procedure allows mixing the synovial fluid with the contrast agent inside the knee joint. The sample was blotted on gauze to absorb excess fluid, and carefully placed in an air-tight tube holder for a quick scan (19.7 μm resolution, 6.5 m duration) to verify the presence and distribution of Microfil in the joint space, and then scanned at high resolution (2.7 μm resolution, 2 h duration, see details below). For the second group of animals ($n = 6$), 1:0 HDM was mixed with 10% volume of hardener (MV curing agent, flowtech Inc) for solidification of the contrast material and injected into the synovial cavity. 1:0 HDM samples were scanned similarly to the LDM group and subsequently processed for histological analysis.

Surgical DMM of the tibiofemoral joint was performed in a third group of animals ($n = 5$) by transecting the meniscotibial ligament (MMTL). The contralateral limb from these animals served as Controls ($n = 5$). Briefly, the joint capsule medial to the patellar tendon is incised and opened to expose the intercondylar region. The MMTL is then transected, leading to DMM. A complete description of the procedure was previously reported in 8–10 week-old male mice[27]. After surgery, animals were allowed unrestricted cage activity, food and water *ad libitum*. Rats were terminated 4 weeks post-surgery and DMM joints were analyzed against Controls (CN).

Scanning, reconstruction and thresholding of μCT images

Knee joints were scanned using a μCT scanner (1172 Skyscan, Belgium) with an isotropic voxel size of 2.7 μm (100 kV, 100 μA, 2 h duration, 10MPixels camera, 11 mm width field of view). X-ray projections were acquired with five averaged exposures to produce high contrast low noise images. A standard reconstruction algorithm (Feldkamp cone beam) was used to generate cross-sectional images using NRecon software (V1.6.1.2, SkyScan, Belgium). Images were compensated for misalignment, ring artifacts and beam hardening during reconstruction of images. Tissue composition and density were calibrated by using density phantoms (250 and 750 mg/cm^3, 7 mm Dia.) of HA, and gray scale reference of air and water. A global threshold value of 450 mgHA/cm^3 was determined by analyzing the 2.7 μm voxel size images using an edge detection algorithm (Canny–Deriche filtering, ImageJ v 1.37, National Institutes of Health).

Histological validation of μCT images

The hardened 1:0 HDM knee joints were fixed in 10% Neutral Buffered Formalin (NBF) at room temperature for 48 h and undecalcified tissues were plastic embedded in Caroplastic. Transverse and sagittal sections were cut at 100 μm thickness, which were found to maintain a reasonable amount of hardened Microfil material. Sections were stained with Trichrome blue for 20 min and digital image of each section was captured by a high-performance color camera (Zeiss Axiocam Mrc). Thirty-four histological sections were randomly selected for the comparison of histological and μCT thickness measurements. Approximately 5,000 μCT images per knee were sequentially reviewed by one operator in DataViewer (SkyScan, Belgium) to identify the image that best matched each histological section. For identification of soft tissues in μCT images, a reverse-contrasting approach was used, in which an inverse threshold was applied to images in order to select all voxels with values above the X-ray absorption of air and below the threshold value used for bone and contrast agent. Thickness analysis regions include patellar-femoral cartilage, femoral cartilage, and medial and lateral tibial cartilage from transverse sections, and patellar-femoral cartilage, femoral-tibial cartilage from sagittal sections. Thickness analysis on both histological and μCT images were performed using the automated 2D thickness analysis operation in CTAn software.

Role of μCT voxel size on cartilage thickness and volume measurements

The role of μCT voxel size (vx) on measurements of cartilage thickness (Cg.Th) and cartilage volume (Cg.V) was investigated by comparing the native resolution (2.7 μm) of the μCT with 15 additional images-datasets at lower resolutions (5.5–44.4 μm). To obtain these measurements, VOIs that included cartilage, subchondral bone and Microfil from the femoral condyle were identified in samples from both the HDM ($n = 6$) and the LDM groups ($n = 6$). Lower resolution images of this VOI were obtained by increasing voxel size by a factor ×2 up to ×16 using CTAn software. Cartilage thickness was calculated via the automated 3D thickness measurement in CTAn. The thickness measurement corresponds to an average measurement of the diameter of multiple spheres which fulfills two conditions: the spheres should enclose a point representing cartilage and the sphere should be entirely bounded within the solid surfaces of the cartilage volume. Cartilage volume was obtained using the 3D volume measurement from CTAn, which uses a hexahedral marching cubes algorithm to determine the number of voxels selected within the thresholded VOI. The total volume was calculated as the total number of cartilage voxels in the VOI times the voxel size in microns cube. The % error in cartilage thickness Cg.Th.%er(vx), and cartilage volume Cg.V.%er(vx), were determined as a function of the voxel size, in respect to measurements at 2.7 μm voxel size (reference value) using the following equations:

$$\mathrm{Cg.Th.\%er}(vx) = \left|\frac{\mathrm{Cg.Th.}(2.7\ \mu\mathrm{m}) - \mathrm{Cg.Th.}(vx)}{\mathrm{Cg.Th.}(2.7\ \mu\mathrm{m})}\right| \times 100$$

$$\mathrm{Cg.V.\%er}(vx) = \left|\frac{\mathrm{Cg.V.}(2.7\ \mu\mathrm{m}) - \mathrm{Cg.V.}(vx)}{\mathrm{Cg.V.}(2.7\ \mu\mathrm{m})}\right| \times 100 \quad ,$$

$$vx = 2.7, 5.4, \ldots, 44.4\ \mu\mathrm{m}.$$

Hard and soft tissues in the DMM model

Newly formed osteophytes (Oph) and cartilage ulcerations were analyzed based on morphological changes and appearance of the underlying bone and cartilage contours in μCT images. For characterization of bone microarchitecture, cylindrical VOIs of 1.5 mm diameter containing bone, cartilage and Microfil were identified in each DMM knee joint ($n = 5$) and in its contralateral CN knee joint ($n = 5$). For each VOI, global architectural parameters such as porosity (φ), trabecular thickness (Tb.Th), trabecular number (Tb.N), and trabecular spacing (Tb.Sp) were measured using built-in algorithms in CTAn software employing the guidelines for

assessment of bone microarchitecture using μCT[28]. Cartilage thickness (Cg.Th) was measured using a methodology similar to trabecular thickness. This analysis was performed in VOIs from four anatomical regions of each joint including the lateral and medial femoral condyles (LFC and MFC), as well as the lateral and medial tibial plateau (LTP, MTP).

Statistical analysis

The correlation between cartilage thicknesses measured by μCT and by histology was calculated using Pearson's correlation coefficient. The effect of voxel size (vx) on cartilage measurements (Cg.Th.%er or Cg.V.%er) was assessed by repeated measures analysis of variance (ANOVA) and Dunnet's post tests on samples measured at different voxel sizes as described above. Analysis of normality indicated that Cg.Th.%er and Cg.V.%er data was normally distributed for all voxel size groups in the HDM knees. However, Cg.Th.%er and Cg.V.%er data were not normally distributed in three of the 16 voxel size groups in LDM joints. Therefore, significant differences among resolutions in the LDM group were assessed using Friedman's test followed by Dunn's post test. Separate analyses were carried out on samples from HDM and LDM joints ($n = 6$ independent samples each, and $m = 16$ repeated observations per independent sample). The effect of surgical DMM on cartilage and bone microarchitecture (trabecular porosity, thickness, number, trabecular spacing, degree of anisotropy, and cartilage thickness) was analyzed by comparing measurements from the DMM group ($n = 5$) with measurements from their respective contralateral CN limbs ($n = 5$), at four anatomical locations (MTP, LTP, MFC, and LFC). Analysis of normality indicated that microarchitecture data was normally distributed for all DMM and CN groups. Two-way repeated measures ANOVA and Bonferroni *post hoc* test were used to compare DMM vs CN data at four anatomical locations. Also, it was investigated whether the source of variation was from DMM treatment and anatomical location, or from the interaction of these two factors.

Prior to performing statistical tests, normality was verified by the Kolmogorov–Smirnov test. Results were expressed as the mean ± 95% confidence interval of the mean (error bars in figures). All tests were performed with $P < 0.05$ significance level using Prism 5 statistics software package (GraphPad Software Inc.).

Results

Contrast agent characterization

Histograms of X-ray absorption intensities for the air, water, 250 and 750 mg/cm^3 HA standards are shown in Fig. 1(A–D), with a distinctive peak at −1000, 0, 2500 and 7500 HU respectively. Fig. 1(F–I) shows the histogram of intensities for the 1:0, 1:1, 1:3 and 1:4 LDM (blue) and HDM (red) dilutions without hardener. The peaks of LDM and HDM at 1:0, 1:1, 1:3 and 1:4 dilutions exhibited X-ray intensities that linearly depend on its concentration within the range tested in this study. Fig. 1(E) shows the histogram of intensities from one knee joint injected with 1:0 LDM. The histogram shows only two distinctive peaks because the X-ray absorption of bone and 1:0 LDM was very similar. When the four LDM dilutions were compared with the absorption by bone, it was observed that the dilution most similar to bone was indeed the 1:0 LDM, corresponding to a HA mass density of ∼1800 mg/cm^3 Fig. 1(J) corresponds to the histogram of intensities from a knee scanned with 1:0 HDM. In this case, three peaks are clearly observed, the one on the left for soft tissues, the one in the middle from hard tissues and the one on the right corresponds to the 1:0 HDM. This indicates that the use of the 1:0 HDM dilution clearly separates bone from the contrast agent. There was no significant difference in intensity when hardener was added to any density or dilution. The use of no hardener has the advantage of using the

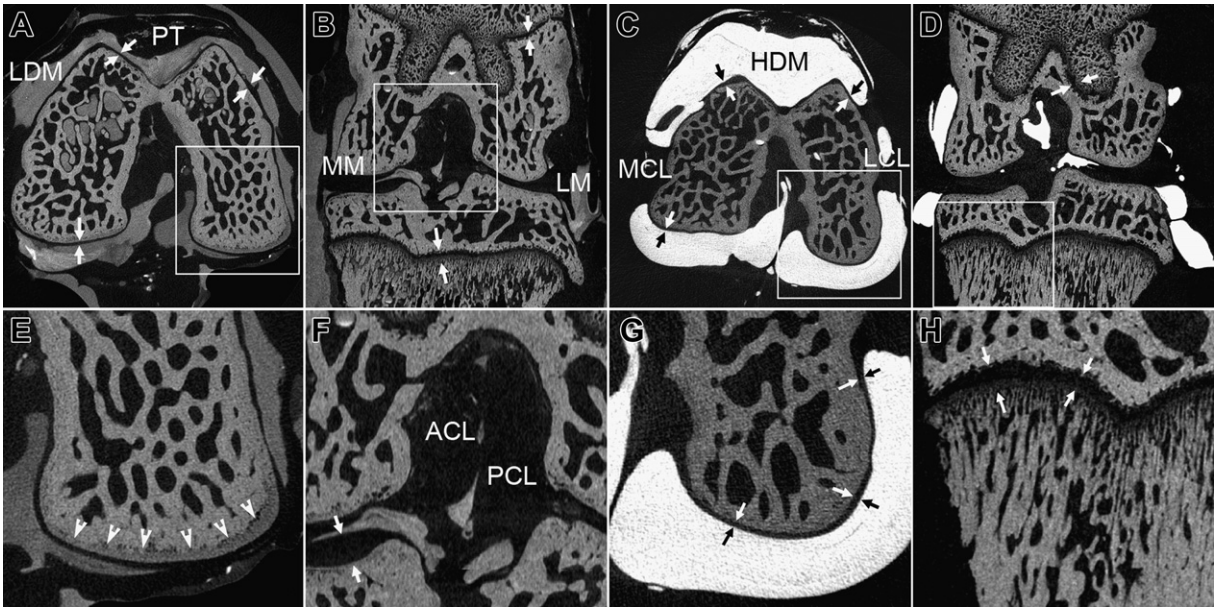

Fig. 2. Contrast enhanced μCT images of a rat knee joint at 2.7 μm voxel size. (A) Transverse plane of 1:0 LDM scan indicating the Patellar Tendon (PT) and femoral cartilage (arrows); inset in panel A showing subchondral bone is magnified in panel E. (B) Coronal plane showing the Medial Meniscus (MM), Lateral Meniscus (LM); and femoral and tibial growth plate; inset in panel B showing a magnified view of Anterior Cruciate Ligament (ACL), Posterior Cruciate Ligament (PCL) and tibial cartilage (arrows) in panel F. (C) Transverse plane of a 1:0 HDM scan showing the Lateral Collateral Ligament (LCL), Medial Collateral Ligament (MCL) and femoral cartilage (arrows); inset in panel C displaying a magnified view of femoral cartilage, subchondral bone and microfil interface in panel G. (D) Coronal plane of a 1:0 HDM scan indicating the Posterior Cruciate Ligament (arrows) and femoral growth plate; inset in panel D showing a magnified view in greater detailed of tibial trabecular bone and growth plate subchondral bone in panel H (arrows).

contrast agent in their liquid form, so that the same knee joint can be bent at different angles and re-scanned; on the contrary, the use of hardener is irreversible, and the knee cannot be flexed/extended any more, but its use facilitates the comparison between histology and the μCT images.

Fig. 2 shows different views of μCT images when the 1:0 LDM and 1:0 HDM were injected into the knee joint. It can be observed that the Microfil was distributed throughout the whole synovial space and did not diffuse into soft or hard tissues. Microfil infiltrated in small spaces including those of cartilage to cartilage interfaces and meniscus to cartilage contact areas. Therefore, Microfil allowed for formation of distinctive boundaries between the synovial fluid space and soft tissues in great detail. Multiple soft tissue anatomical structures not easily seen by standard μCT were discriminated including menisci, ligaments, cartilages, and tendons. Overall, the HDM contrast agent in Fig. 2(C and D) help to more easily distinguish/separate the soft tissues in the knee by thresholding procedures because of the remarkable HU-intensity peak separations.

Histology vs μCT images

Fig. 3(A and B) shows a sagittal histological section and μCT image of the knee joint in which hardened 1:0 HDM, bone, and cartilage can be clearly distinguished. The corresponding histological sections stained with Trichrome blue demonstrated a high resemblance with μCT images [highlighted in Fig. 3(C and D)]. Quantitative comparison of cartilage thickness from histological and μCT sections using in both cases the CTAn automated image analysis yield a correlation value of 0.90 [Fig. 3(E)], indicating that cartilage measurements from μCT images with Microfil appropriately represent the true thickness of cartilage in small joints at this resolution.

Effect of image resolution

A qualitative comparison of images at different resolutions (2.7 μm–88.3 μm) with 1:0 LDM and 1:0 HDM is shown in Fig. 4(A and B) respectively. This sequence of images shows that the cartilage layer can still be distinguished at 22.1 μm, but its clarity is strongly compromised below that resolution, as shown in panels at 44.2 μm and 88.3 μm pixel size (typical MRI resolution). Moreover, we quantitatively analyzed the role of the voxel size on the % error produced on cartilage measurements. The cartilage thickness and volume was determined at 16 different resolutions and plotted as a function of the voxel size in Fig. 4(C and D). The % error of the cartilage thickness and volume measurements increases linearly with voxel size, and at 22.1 μm was found to be ~30% and ~4% respectively. Above 44.2 μm voxel size the thickness % error was as large as 60%, possibly because the cartilage thickness was represented by a few pixels at that resolution. No significant differences from Cg.Th.%er measured at 2.7 μm were found until voxel size reached 13.8 μm or higher in HDM samples. Cg.Th.%er measured from LDM samples was significantly different when comparing 2.7 μm–11.1 μm and higher voxel sizes. No significant differences were found for Cg.V.%er at 24.9 μm and smaller voxel sizes in HDM samples, and at 22.1 μm and smaller voxel sizes in LDM samples. All together, these results highlight the importance of resolution on quantitative assessment of cartilage thickness and volume.

Assessment of changes in DMM animal model

Fig. 5(A) shows the DMM 4 weeks after surgery, in which the medial meniscus was medially displaced, allowing a greater contact

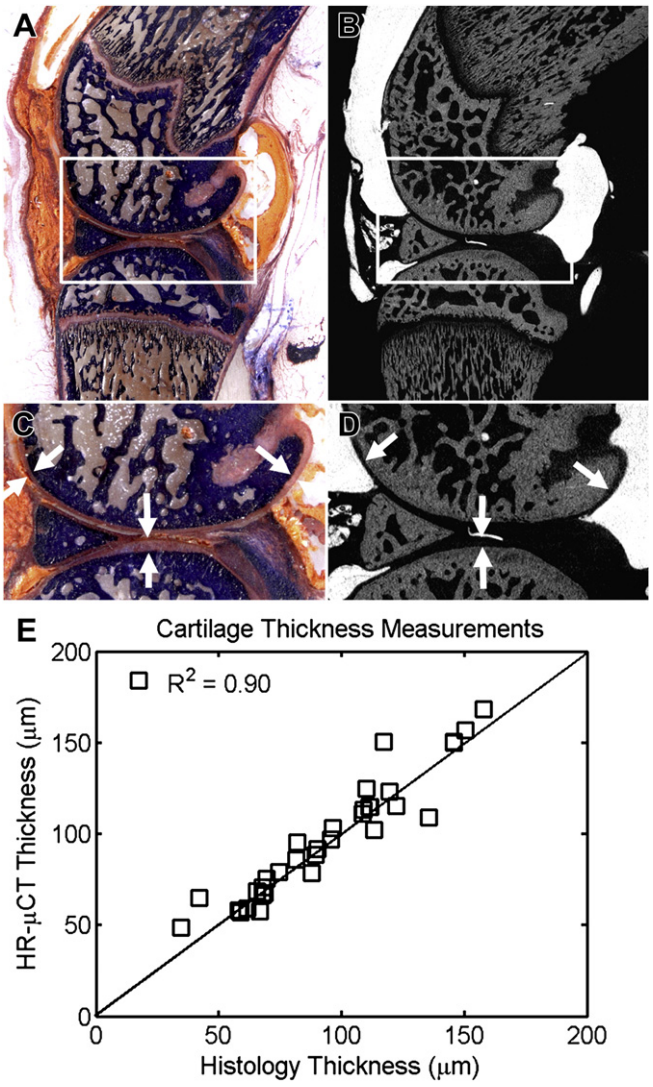

Fig. 3. Comparison among structures and thickness measurements of μCT and histological images. Corresponding sagittal view of (A) histology and (B) μCT images of the same knee joint. (C) Magnified view of inset in panel A, indicating bone (blue), HDM contrast agent (orange) and cartilage (light pink). (D) Magnified view of inset area shown in panel B, indicating bone (gray color), HDM contrast agent (light gray) and cartilage (black). White arrows indicate the cartilage in all images. (E) Pearson's correlation coefficient between histology and μCT cartilage thickness was found $R^2 = 0.90$ with a slope of 0.97.

between the femoral condyle and tibial plateau in the medial compartment of the knee joint. Several changes in trabecular bone and cartilage can be observed in the DMM group, including the formation of Oph in both the tibia [Fig. 5(A and E)] and femur [Fig. 5(B and F)], as well as erosion and ulceration of the cartilage layer in the tibia [Fig. 5(C and G)] and the femur [Fig. 5(D and H)] as indicated with white arrowheads. None of these changes were observed in the control group.

Changes on trabecular bone microarchitecture and cartilage thickness due to surgical DMM are summarized in Fig. 6. A pattern of change on porosity can be observed on each of the four compartments of the tibiofemoral joint, characterized by a small increase of the mean on each DMM group vs Control [Fig. 6(A)]. The effect of DMM on porosity changes was found extremely significant. However, the effect of location was found not quite significant and the interaction between DMM and location was found not significant. The *post hoc* test showed that the change in porosity was

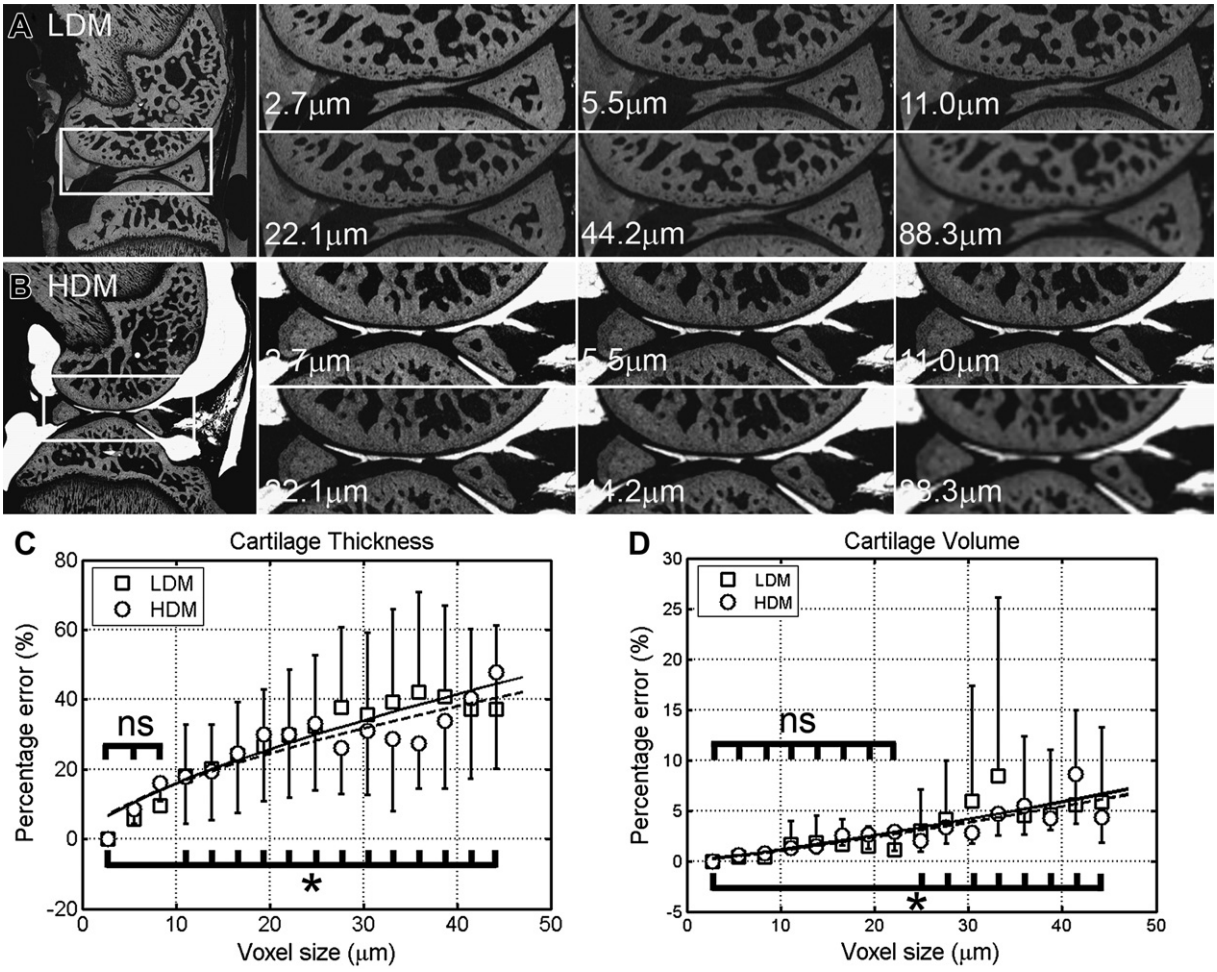

Fig. 4. Single sagittal slice of μCT images with LDM ($n = 6$) and HDM ($n = 6$) at resolutions of 2.7, 11.0, 22.1, 44.2, and 88.3 μm voxel size. (A) Demonstrating the effect of resolution on the ability to resolve tissues and structures in the knee joint injected with 1:0 LDM. At 44-μm voxel size, the tissues boundaries are blurred owing to partial volume effect so that the gray scale is sufficiently reduced to the extent that they cannot be differentiated from each other. Same partial volume effect is seen on (B) however knee joint was injected with 1:0 HDM. Quantitative assessment (mean ± 95% CI shown as error bars) of cartilage thickness % error (C) and cartilage volume % error (D) as a function of voxel size (16 repeated observations per independent sample).

found statistically significant only in the MFC region. The effect of interaction of these two factors on porosity was found not significant .A similar observation was obtained for trabecular thickness, which has the opposite trend to the one displayed by the porosity [Fig. 6(B)]. The effect of DMM on Tb.Th. was considered extremely significant, the effect of location was significant, but the interaction was not significant. These changes were found statistically significant by the *post hoc* test in the MTP, LTP and MFC regions. The trabecular spacing followed a pattern close to the one showed in the porosity, in which DMM treatment and location, but not the

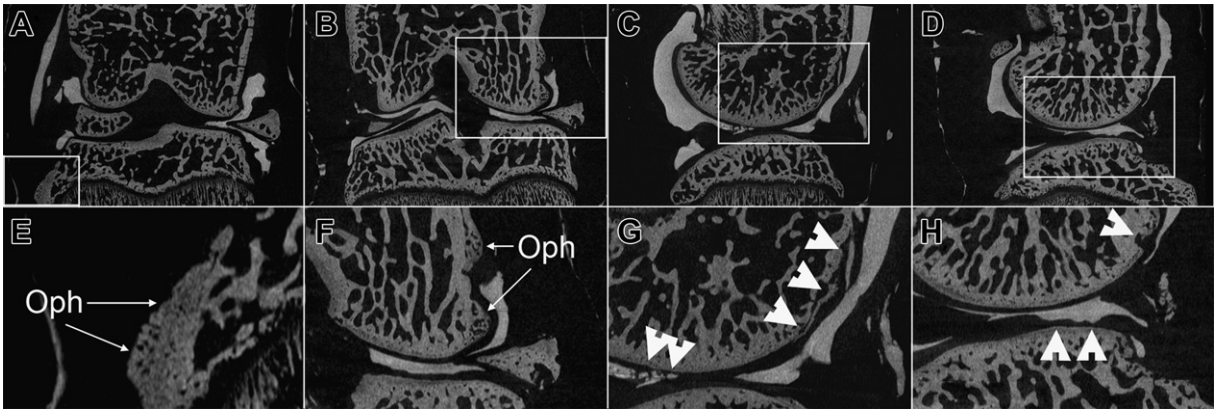

Fig. 5. Contrast enhanced μCT images of tibiofemoral joints after surgical destabilization of medial meniscus. (A and B) Coronal plane displaying the medial meniscus out of place. (C and D) sagittal views of the DMM model showing ulceration and erosion of tibial and femoral cartilage respectively. (E and F) Magnified views of A and B showing the formation of Oph in the tibia and femur. (G and H) disruption and ulceration of femoral and tibial cartilage.

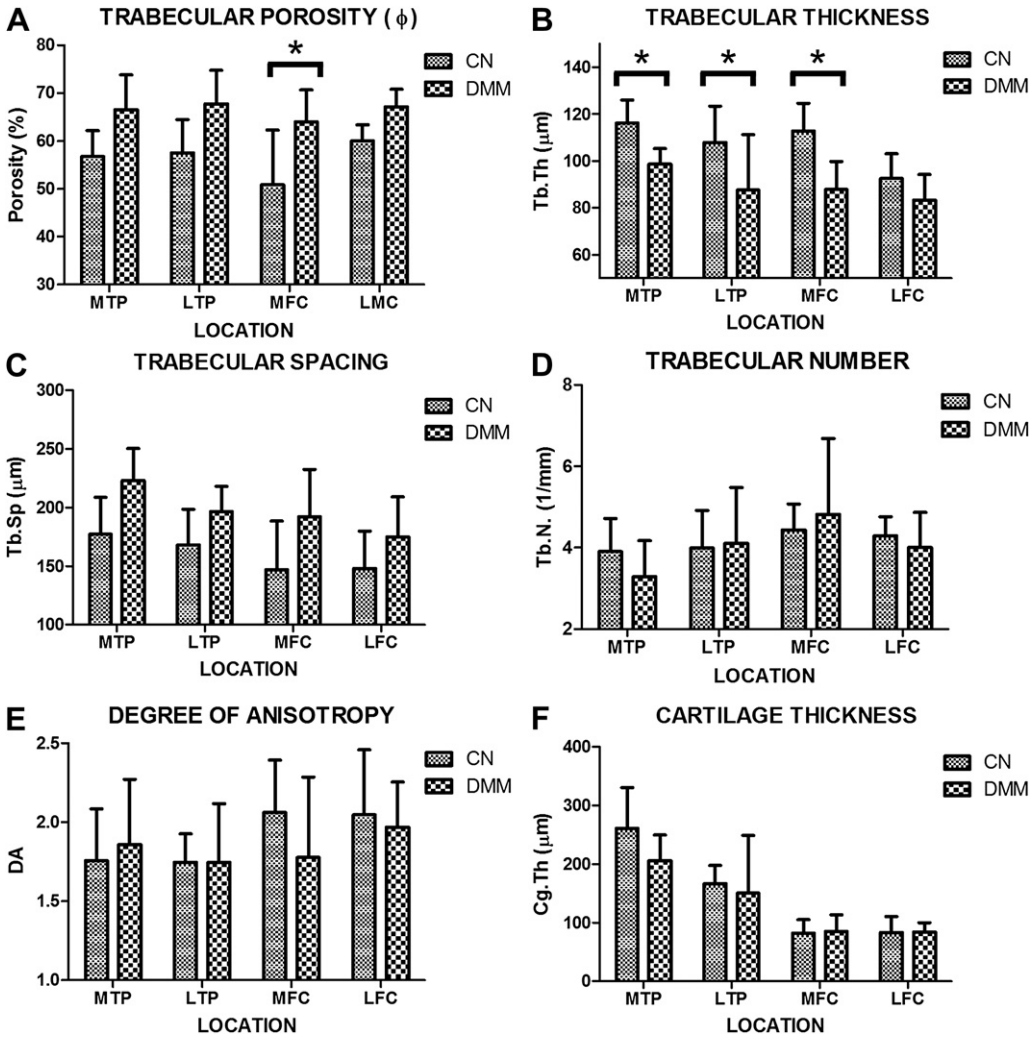

Fig. 6. Characterization of bone microarchitecture and cartilage thickness at four distinct compartments (LFC, LTP, MFC, and MTP) of the tibiofemoral joint from DMM ($n = 5$) and CN ($n = 5$) groups. (A) trabecular porosity (ϕ), (B) trabecular number (Tb.N), (C) trabecular thickness (Tb.Th), (D) trabecular spacing (Tb.Sp), (E) degree of anisotropy (DA), and F) cartilage thickness (Cg.Th). Data shown as mean ± 95 confidence interval (error bars), * indicates significant differences between groups with $P < 0.05$ level, ns indicates non significant differences.

interaction between these factors, had a very significant effect on Tb.Sp. However, the *post hoc* test indicated that no significant differences were found among the groups [Fig. 6(C)]. The trabecular number and the degree of anisotropy seem to be the less affected by the surgical DMM procedure [Fig. 6(D and E)] since these two parameters exhibited no effect by DMM treatment, location or interaction between these factors. *Post hoc* test showed no significant differences among the analyzed groups. The cartilage thickness measurements indicate that DMM and the interaction between DMM and location had no effect on Cg.Th, however, location had a very significant effect on Cg.Th. *Post hoc* test showed no differences among groups [Fig. 6(F)].

Discussion

Quantitative characterization of hard tissues has become a standard procedure in many laboratories equipped with μCT systems. Assessment of 3D changes in soft tissues in small animal models is being currently developed with the help of contrast agents, which has the potential to become a (semi)automated procedure too. A suspension of barium sulfate in oil was employed to distinguish the synovial fluid from the cartilage anatomy imaged by μCT arthrography at 35 μm resolution[29]. Equilibrium Partitioning of an Ionic Contrast agent via μCT (EPIC-μCT) using Hexabrix at 16 μm resolution was proved efficient for imaging GAG content and thus to quantify tissue composition, which is indicative of the healthy state of cartilage[26,30,31,32]. Other cationic contrast agents have also shown great sensitivity to GAG content[33,34]. In both methods, using either anionic or cationic contrasts, the contrast agent diffuses across the soft tissues surface, until equilibrium is reached between the contrast agent concentration inside cartilage and the synovial space. Therefore, a clear distinction between the soft tissue interface and the synovial fluid may be difficult to achieve. In the contrary, Microfil does not diffuse across the border of the soft tissues, and the delineation of soft tissues, which is difficult in μCT, becomes quantifiable due to the enhanced contrast at the interface between soft tissues and synovial fluid space. The high contrast between tissues and Microfil made possible distinguishing with clarity the morphology of both hard and soft tissues in scans with 22 μm pixel size or smaller. To the best of authors' knowledge, this contrast agent has not been used before for characterization of soft tissues within a whole intact knee joint. Further studies are required to investigate whether Hexabrix and Microfil may be used synergistically to assess changes in tissue composition and morphology.

Another important advantage of Microfil is that it enables automated segmentation of hard and soft tissues in the knee joint (Fig. 2). The contrast agent concentration may be tuned to exhibit a desired/convenient X-ray absorption in the scan. For instance, the use of 1:0 HDM offers the advantage of producing three distinctive peaks in the attenuation histogram of images [Fig. 1(J)], thus facilitating the segmentation of tissues and the compartment occupied by the contrast agent in the knee joint. In this manner, a single imaging approach can be used for characterization of both hard and soft tissues, as opposed to previous studies requiring the assessment of hard tissues by μCT and soft tissues by MRI.

In all scans performed in this study, the volume of the contrast agent represented fairly well the synovial fluid cavity and revealed the anatomical details of the soft tissues in the intra-articular space. In order to assess the accuracy of this approach to quantify soft tissue morphology, we analyzed the cartilage thickness obtained from histological sections and μCT images (2.7 μm pixel size) using CTAn automated software. A strong linear relationship between the μCT thickness measures and histology was observed ($R^2 = 0.90$, slope = 0.97), demonstrating the utility of Microfil to quantify cartilage morphology at high resolution (Fig. 3). By using the automated thickness analysis operation in CTAn, human measurement errors were minimized. However, a limitation of this approach is that the use of histological slices (and 2D image slices) could be influenced by the 3D nature of the joints, and a small misalignment could be a source of error.

Measurements of cartilage volume are possible due to the successful segmentation and 3D reconstructions of both hard and soft tissues. The analysis of the influence of the pixel size on the quantitative assessment of cartilage thickness and volume indicated that there is a moderate error on such measurements when performed on scans at 22.1 μm pixel size or smaller (<30% and 4% respectively). When the pixel size is as large as the cartilage thickness, these measurements exhibited an error of up to 60%. Scans with 2.7 μm isotropic voxel size indeed offered outstanding recognizable details of both hard and soft tissues. A limitation of this analysis is that generating image datasets with reduced resolution by averaging techniques is not exactly the same as performing the measurements independently at varying resolutions, but it is considered as a reasonable approach to address the question of resolution effects on accuracy.

The use of Microfil also allowed the simultaneous characterization of trabecular bone microarchitecture, as well as the development of Oph and cartilage ulcerations 4 weeks after surgical DMM. Distinguishing the boundary of cartilage is important to quantify the morphological changes associated with cartilage degeneration such as thickening/thinning, erosion, and ulceration. A more extensive characterization (including more animals and other time points) of the DMM model is necessary to confirm the findings reported here. A limitation of the lead chromate contrast agent is that it could be toxic to the animal, limiting the applicability of this contrast agent *in vivo*; however, the concept of using a contrast agent that does not diffuse across the soft tissues is of relevance to translate the proposed approach to *in vivo* animal models. However, the possibility of tracking changes in both soft and hard tissues *ex vivo* with the level of detail presented in this study may contribute to better understand the interaction between soft and hard tissues in joint diseases and therapeutic interventions, i.e. osteoarthritis, post surgery soft tissue healing, surgical DMM, etc.

Contributions

Role of authors: Study conception and design: XIG, PEPM, RJM, MBS, HBS & LC. Acquisition of data: XIG, PEPM, YB, EW & DL. Analysis and interpretation of data: XIG, PEPM, DJL, MN, YHL, DL, RJM, MBS, HBS & LC. All authors were involved with the drafting and revising of the manuscript as well as having approved the manuscript for publication. XIG (ian_guxiang1@yahoo.com), PEPM (paolopalacio@gmail.com) and LC (cardoso@engr.ccny.cuny.edu) take responsibility for the integrity of this work from inception to the finished manuscript.

Role of the funding sources

This project was funded by the National Science Foundation (NSF 0723027) and National Institutes of Health (AG34198 & HL069537-07 R25 Grant for Minority BME Education) and by a Science Fellowship from The City University of New York.

Conflict of interest

None of the authors declare any competing interests in relation to this study.

Acknowledgments

This work was supported by grants from The City University of New York (Science Fellowship), the National Science Foundation (NSF 0723027) and National Institutes of Health (AG34198 & HL069537-07 R25 Grant for Minority BME Education). The authors are grateful to Dr Susannah Fritton, Dr Bingmei Fu, Dr David Rumschitzki and their lab members Dr Min Zeng, Bin Cai, Jie Fan, Lingyan Shi, Ling Zhang, Guangeli Li, Wei Yuan, Yan Xue, and Qin Liu at the City College of New York.

References

1. Goldring SR, Goldring MB. Clinical aspects, pathology and pathophysiology of osteoarthritis. J Musculoskelet Neuronal Interact 2006;6:376–8.
2. Buckwalter JA, Martin J, Mankin HJ. Synovial joint degeneration and the syndrome of osteoarthritis. Instr Course Lect 2000;49:481–9.
3. Goldring SR. Role of bone in osteoarthritis pathogenesis. Med Clin North Am 2009;93:25–35, doi:10.1016/j.mcna.2008.09.006. xv, S0025-7125(08)00134-X [pii].
4. Bellido M, Lugo L, Roman-Blas JA, Castañeda S, Caeiro JR, Dapia S, *et al.* Subchondral bone microstructural damage by increased remodelling aggravates experimental osteoarthritis preceded by osteoporosis. Arthritis Res Ther 2010;12:R152, doi:10.1186/ar3103. ar3103 [pii].
5. Blain EJ, Mason DJ, Duance VC. The effect of cyclical compressive loading on gene expression in articular cartilage. Biorheology 2003;40:111–7.
6. Wu JZ, Herzog W, Epstein M. Joint contact mechanics in the early stages of osteoarthritis. Med Eng Phys 2000;22:1–12. http://dx.doi.org/10.1016/S1350-4533(00)00012-6 [pii].
7. Brosseau L, Milne S, Wells G, Tugwell P, Robinson V, Casimiro L, *et al.* Efficacy of continuous passive motion following total knee arthroplasty: a metaanalysis. J Rheumatol 2004;31:2251–64.
8. Salter RB. The physiologic basis of continuous passive motion for articular cartilage healing and regeneration. Hand Clin 1994;10:211–9.
9. Ferretti M, Gassner R, Wang Z, Perera P, Deschner J, Sowa G, *et al.* Biomechanical signals suppress proinflammatory responses in cartilage: early events in experimental antigen-induced arthritis. J Immunol 2006;177:8757–66. 177/12/8757 [pii].
10. Ferretti M, Srinivasan A, Deschner J, Gassner R, Baliko F, Piesco N, *et al.* Anti-inflammatory effects of continuous passive motion on meniscal fibrocartilage. J Orthopaedic Res 2005;23:1165–71. http://dx.doi.org/10.1016/j.orthres.2005.01.025.

11. Gu XI, Leong DJ, Guzman F, Mahamud R, Li YH, Majeska RJ, *et al*. Development and validation of a motion and loading system for a rat knee joint in vivo. Ann Biomed Eng 2010;38:621–31. http://dx.doi.org/10.1007/s10439-009-9865-0.
12. Leong DJ, Gu XI, Li Y, Lee JY, Laudier DM, Majeska RJ, *et al*. Matrix metalloproteinase-3 in articular cartilage is upregulated by joint immobilization and suppressed by passive joint motion. Matrix Biol 2010;29(5):420–6. S0945-053X(10)00031-4 [pii], http://dx.doi.org/10.1016/j.matbio.2010.02.004.
13. Dorr LD. Continuous passive motion offers no benefit to the patient. Orthopedics 1999;22:393.
14. Leong DJ, Li YH, Gu XI, Sun L, Zhou Z, Nasser P, *et al*. Physiological loading of joints prevents cartilage degradation through CITED2. FASEB J 2011;25:182–91, doi:10.1096/fj.10-164277. fj.10-164277 [pii].
15. Andriacchi TP, Lang PL, Alexander EJ, Hurwitz DE. Methods for evaluating the progression of osteoarthritis. J Rehabil Res Dev 2000;37:163–70.
16. Eckstein F, Tieschky M, Faber S, Englmeier KH, Reiser M. Functional analysis of articular cartilage deformation, recovery, and fluid flow following dynamic exercise in vivo. Anat Embryol (Berl) 1999;200:419–24. http://dx.doi.org/10.1007/s004290050291 92000419.429 [pii].
17. Guermazi A, Eckstein F, Hellio Le Graverand-Gastineau MP, Conaghan PG, Burstein D, Keen H, *et al*. Osteoarthritis: current role of imaging. Med Clin North Am 2009;93:101–26, doi:10.1016/j.mcna.2008.08.003. xi, S0025-7125(08)00121-1 [pii].
18. Goebel JC, Bolbos R, Pinzano A, Schaeffer M, Rengle A, Galois L, *et al*. In vivo rat knee cartilage volume measurement using quantitative high resolution MRI (7 T): feasibility and reproducibility. Biomed Mater Eng 2008;18:247–52.
19. Rengle A, Armenean M, Bolbos R, Goebel JC, Pinzano-Watrin A, Saint-Jalmes H, *et al*. A dedicated two-channel phased-array receiver coil for high-resolution MRI of the rat knee cartilage at 7 T. IEEE Trans Biomed Eng 2009;56:2891–7, doi:10.1109/TBME.2008.2006015.
20. Koo S, Giori NJ, Gold GE, Dyrby CO, Andriacchi TP. Accuracy of 3D cartilage models generated from MR images is dependent on cartilage thickness: laser scanner based validation of in vivo cartilage. J Biomech Eng 2009;131:121004, doi:10.1115/1.4000087.
21. Koo S, Gold GE, Andriacchi TP. Considerations in measuring cartilage thickness using MRI: factors influencing reproducibility and accuracy. Osteoarthritis Cartilage 2005;13:782–9, doi:10.1016/j.joca.2005.04.013. S1063-4584(05)00111-1 [pii].
22. Haubner M, Eckstein F, Schnier M, Lösch A, Sittek H, Becker C, *et al*. A non-invasive technique for 3-dimensional assessment of articular cartilage thickness based on MRI. Part 2: validation using CT arthrography. Magn Reson Imaging 1997;15:805–13. http://dx.doi.org/10.1016/S0730-725X(97)00011-8 [pii].
23. Adams Jr SB, Herz PR, Stamper DL, Roberts MJ, Bourquin S, Patel NA, *et al*. High-resolution imaging of progressive articular cartilage degeneration. J Orthop Res 2006;24:708–15, doi:10.1002/jor.20083.
24. Patel NA, Zoeller J, Stamper DL, Fujimoto JG, Brezinski ME. Monitoring osteoarthritis in the rat model using optical coherence tomography. IEEE Trans Med Imaging 2005;24:155–9. http://dx.doi.org/10.1109/TMI.2004.839360.
25. Roberts MJ, Adams Jr SB, Patel NA, Stamper DL, Westmore MS, Martin SD, *et al*. A new approach for assessing early osteoarthritis in the rat. Anal Bioanal Chem 2003;377:1003–6, doi:10.1007/s00216-003-2225-2.
26. Xie L, Lin AS, Levenston ME, Guldberg RE. Quantitative assessment of articular cartilage morphology via EPIC-microCT. Osteoarthritis Cartilage 2009;17:313–20, doi:10.1016/j.joca.2008.07.015. S1063-4584(08)00263-X [pii].
27. Glasson SS, Blanchet TJ, Morris EA. The surgical destabilization of the medial meniscus (DMM) model of osteoarthritis in the 129/SvEv mouse. Osteoarthritis Cartilage 2007;15:1061–9, doi:10.1016/j.joca.2007.03.006. S1063-4584(07)00110-0 [pii].
28. Bouxsein ML, Boyd SK, Christiansen BA, Guldberg RE, Jepsen KJ, Müller R. Guidelines for assessment of bone microstructure in rodents using micro-computed tomography. J Bone Miner Res 2010;25:1468–86, doi:10.1002/jbmr.141.
29. Roemer FW, Mohr A, Lynch JA, Meta MD, Guermazi A, Genant HK. Micro-CT arthrography: a pilot study for the ex vivo visualization of the rat knee joint. AJR Am J Roentgenol 2005;184:1215–9.
30. Palmer AW, Guldberg RE, Levenston ME. Analysis of cartilage matrix fixed charge density and three-dimensional morphology via contrast-enhanced microcomputed tomography. Proc Natl Acad Sci USA 2006;103:19255–60, doi:10.1073/pnas.0606406103.
31. Piscaer TM, Waarsing JH, Kops N, Pavljasevic P, Verhaar JA, van Osch GJ, *et al*. In vivo imaging of cartilage degeneration using muCT-arthrography. Osteoarthritis Cartilage 2008;16:1011–7, doi:10.1016/j.joca.2008.01.012. S1063-4584(08)00025-3 [pii].
32. Xie L, Lin AS, Guldberg RE, Levenston ME. Nondestructive assessment of sGAG content and distribution in normal and degraded rat articular cartilage via EPIC-microCT. Osteoarthritis Cartilage 2009;18:65–72. S1063-4584(09)00203-9 [pii], http://dx.doi.org/10.1016/j.joca.2009.07.014.
33. Bansal PN, Joshi NS, Entezari V, Malone BC, Stewart RC, Snyder BD, *et al*. Cationic contrast agents improve quantification of glycosaminoglycan (GAG) content by contrast enhanced CT imaging of cartilage. J Orthop Res. 2011;29:704–9. http://dx.doi.org/10.1002/jor.21312.
34. Joshi NS, Bansal PN, Stewart RC, Snyder BD, Grinstaff MW. Effect of contrast agent charge on visualization of articular cartilage using computed tomography: exploiting electrostatic interactions for improved sensitivity. J Am Chem Soc 2009;131:13234–5, doi:10.1021/ja9053306.